

Locally Sparse Networks for Interpretable Predictions

Junchen Yang^{1*} Ofir Lindenbaum^{1*}
Yuval Kluger^{1†}

¹Yale University, USA; [†]Corresponding author. E-mail: yuval.kluger@yale.edu

Address: 333 Cedar St, New Haven, CT 06510, USA

* These authors contributed equally.

Abstract

Despite the enormous success of neural networks, they are still hard to interpret and often overfit when applied to low-sample-size (LSS) datasets. To tackle these obstacles, we propose a framework for training locally sparse neural networks where the local sparsity is learned via a sample-specific gating mechanism that identifies the subset of most relevant features for each measurement. The sample-specific sparsity is predicted via a *gating* network, which is trained in tandem with the *prediction* network. By learning these subsets and weights of a prediction model, we obtain an interpretable neural network that can handle LSS data and can remove nuisance variables, which are irrelevant for the supervised learning task. Using both synthetic and real-world datasets, we demonstrate that our method outperforms state-of-the-art models when predicting the target function with far fewer features per instance.

1 Introduction

Deep neural networks are becoming prevalent in almost any task in machine learning. The tremendous success of these complex models may be explained by an increase in data size, computational resources that enable deeper models [1, 2], or by implicit properties of the optimization tools [3, 4]. Nonetheless, deep nets suffer from two drawbacks: (1) they are hard to interpret due to non-linearity and over-parameterization (2) they tend to overfit when applied to low-sample-size (LSS) data [5, 6], which are either high dimensional or contain nuisance features. This study proposes locally

sparse neural networks, which as we demonstrate provide an end-to-end solution to (1) and (2).

Interpretability is a critical aspect in machine learning; it is imperative in medicine or biology, where practitioners often do not trust predictions that lack an explanation. Recently, there has been a growing interest in interpretation algorithms that aim to shed light on black box deep nets. Methods such as [7, 8, 9] evaluate the gradients or use perturbations to identify which input features are essential for predictions. Alternatively, neural nets could be explained by assessing the contribution of each training sample to the prediction [10, 9, 11].

In bioinformatics or medicine, datasets are often high-dimensional with a low sample size (HDLSS). HDLSS makes data analysis tasks such as dimensionality reduction [12, 13, 14] challenging. Also, HDLSS poses a key challenge in supervised learning since prediction models tend to overfit [15, 16] when the problem becomes underdetermined. Training deep nets is especially challenging in this regime as a vast amount of parameters leads to a large variance of the gradient estimates [5]. To prevent overfitting in deep nets, several authors [17, 18, 19, 20] have proposed to apply different regularization schemes to sparsify the input features. Alternatively, linear models such as [21, 22, 23, 24] could be used to identify the subset of most informative features.

This study presents Locally SParse Interpretable Networks (LSPIN), a method for fitting predictive models to LSS data. LSPIN is a flexible prediction model that relies on local (sample-specific) sparsity of the input features. To learn the local sparsity, we train a *gating* network to predict the probabilities of the instance-wise *gates* being active. The parameters of the local gates, along with the model coefficients, are learned in tandem by minimizing a classification or regression loss. Our parametric construction leads to an interpretable model which relies on a subset of the input features for each instance. We show via extensive synthetic simulations that our model, albeit its simplicity, can learn the correct target function and identify the informative variables while requiring a small number of observations. Next, we demonstrate that local sparsity, with a linear model can outperform state-of-the-art methods when applied to real biological classification and regression tasks.

Notation: Scalars are denoted by lower case letters x , while vectors are denoted by bold lowercase letters \mathbf{x} . Random variables are represented using normal text x , and random vectors are bold normal text \mathbf{x} . A set is represented by a script font \mathcal{S} . The i^{th} vector-valued observation is denoted as $\mathbf{x}^{(i)}$ whereas $x_d^{(i)}$ represents the d^{th} feature of the i^{th} vector-valued observations. Let $[D] = 1, 2, \dots, D$. For a set $\mathcal{S} \subset [D]$ let the vector $\mathbf{s} \in \{0, 1\}^D$ be the characteristic function for the set. That is $s_i = 1$ if $i \in \mathcal{S}$ and 0 otherwise. For two vectors \mathbf{x} and \mathbf{z} we denote $\mathbf{x} \odot \mathbf{z}$ to be the element-wise

product between \mathbf{x} and \mathbf{z} . The ℓ_1 norm of \mathbf{x} is denoted by $\|\mathbf{x}\|_1 = \sum_{i=1}^D |x_i|$. Finally, the ℓ_0 norm of \mathbf{x} is denoted by $\|\mathbf{x}\|_0$ and counts the total number of non-zero entries in the vector \mathbf{x} .

2 Problem Setup and Method

Let $\mathcal{X} \subset \mathbb{R}^D$ be the observation domain with corresponding target domain \mathcal{Y} (which is continuous for regression and discrete for classification). Given realizations $\{\mathbf{x}^{(i)}, y^{(i)}\}_{i=1}^N$ from the data distribution $P_{X,Y}$, our goal is to learn a prediction model $f_{\boldsymbol{\theta}} \in \mathcal{F}$ which leads to:

1. Small generalization error even in extreme cases of $N < D$.
2. Removal of nuisance variables whose inclusion could be detrimental for predictions.
3. Interpretable predictions.

To address these goals, we propose a model with local sparsity such that predictions are only based on a small subset of features $\mathcal{S}^{(i)} \subset [D], i = 1, \dots, N$ which is optimized for each sample individually. By forcing $|\mathcal{S}^{(i)}| \ll D$, we can reduce the generalization gap of the model and use the (sample-specific) subset of selected features to interpret the prediction model.

2.1 Locally Sparse Predictor

We propose to learn a prediction model with local sparsity. Given observations $\{\mathbf{x}^{(i)}, y^{(i)}\}_{i=1}^N$, with $\mathbf{x}^{(i)} \in \mathbb{R}^D$, our goal is to learn a function $f_{\boldsymbol{\theta}}$ and sets of indicator vectors $\mathbf{s}^{(i)} \in \{0, 1\}^D$ by minimizing the following empirical regularized risk

$$\sum_{i=1}^N \|f_{\boldsymbol{\theta}}(\mathbf{x}^{(i)} \odot \mathbf{s}^{(i)}) - y^{(i)}\|_2 + \lambda \sum_{i=1}^N \|\mathbf{s}^{(i)}\|_0, \quad (1)$$

where λ is a regularization parameter that controls the sparsity level of the model. Due to the discrete nature of the ℓ_0 regularizer, this objective is not differentiable and finding the exact solution of the problem becomes intractable.

2.2 Probabilistic Reformulation

Recently, several authors have demonstrated that the ℓ_0 norm can be relaxed using a probabilistic counterpart. Specifically, by replacing the binary deterministic vector \mathbf{s}

with a Bernoulli vector $\tilde{\mathbf{s}}$, with independent entries which satisfy $\mathbb{P}(\tilde{s}_d = 1) = \pi_d$ for $d \in [D]$. Next, by taking the expectation of the ℓ_0 norm of $\tilde{\mathbf{s}}$, we observe that the term $\mathbb{E}_{\tilde{\mathbf{s}}} \|\tilde{\mathbf{s}}\|_0$ boils down to the sum of Bernoulli parameters $\sum_{d=1}^D \pi_d$. This probabilistic formulation converts the combinatorial search (over the discrete space of $\mathbf{s} \in \{0, 1\}^D$) to a search over the continuous space of Bernoulli parameters ($\boldsymbol{\pi} \in [0, 1]^D$). This formulation becomes useful in several applications such as: model compression [25], feature selection [20], discrete softmax [26], sparse canonical correlation analysis [27] and many more.

By replacing the deterministic vectors \mathbf{s}_i in Eq. 1 with their probabilistic counterparts $\tilde{\mathbf{s}}_i$ we can derive a differentiable loss term. To differentiate a loss which includes discrete random variables we can use solutions such as REINFORCE [28] or the straight-through estimator [29], however, they suffer from a high variance and require many Monte Carlo samples [30]. Alternatively, as demonstrated in [31, 26, 32] a continuous reparametrization of the discrete random variables can reduce the variance of the gradient estimates. Here, we propose to extend the construction in [20], by proposing a Gaussian based reparametrization for the gates vectors \mathbf{s} .

2.3 Local Stochastic Gates

We propose to learn sample-specific gates which will sparsify the model locally. Each gate is defined based on the following hard thresholding function

$$z_d^{(i)} = \max(0, \min(1, 0.5 + \mu_d^{(i)} + \epsilon_d^{(i)})),$$

where $\epsilon_d^{(i)}$ is drawn from $\mathcal{N}(0, \sigma^2)$ and σ is fixed throughout training. The exact choice of σ is discussed in Section B in the Appendix. The sample-specific parameter $\mu_d^{(i)}$ is learned via a *gating* network simultaneously to learn the weights of the networks by minimizing the following loss:

$$\sum_{i=1}^N \mathbb{E}_{z^{(i)}} \|f_{\boldsymbol{\theta}}(\mathbf{x}^{(i)} \odot \mathbf{z}^{(i)}) - y^{(i)}\|_2 + \lambda \sum_{i=1}^N \mathbb{E}_{z^{(i)}} \|\mathbf{z}^{(i)}\|_0, \quad (2)$$

where the sum in the right term is parametric and can be rewritten as:

$$\sum_{i=1}^N \sum_{d=1}^D \mathbb{P}(z_d^{(i)} > 0) = \sum_{i=1}^N \sum_{d=1}^D \left(\frac{1}{2} - \frac{1}{2} \operatorname{erf} \left(-\frac{\mu_d^{(i)} + 0.5}{\sqrt{2}\sigma} \right) \right),$$

and the left term is estimated using Monte Carlo sampling. Following [20], we also observe that one Monte Carlo sample is efficient for gradient estimation. Note that the set of parameters $\boldsymbol{\mu}^{(i)}$, $i = 1, \dots, N$ are predicted based on a *gating* network Ψ such that $\boldsymbol{\mu}^{(i)} = \boldsymbol{\psi}(\mathbf{x}^{(i)} | \boldsymbol{\Omega})$, where $\boldsymbol{\Omega}$ are the weights of the *gating* network.

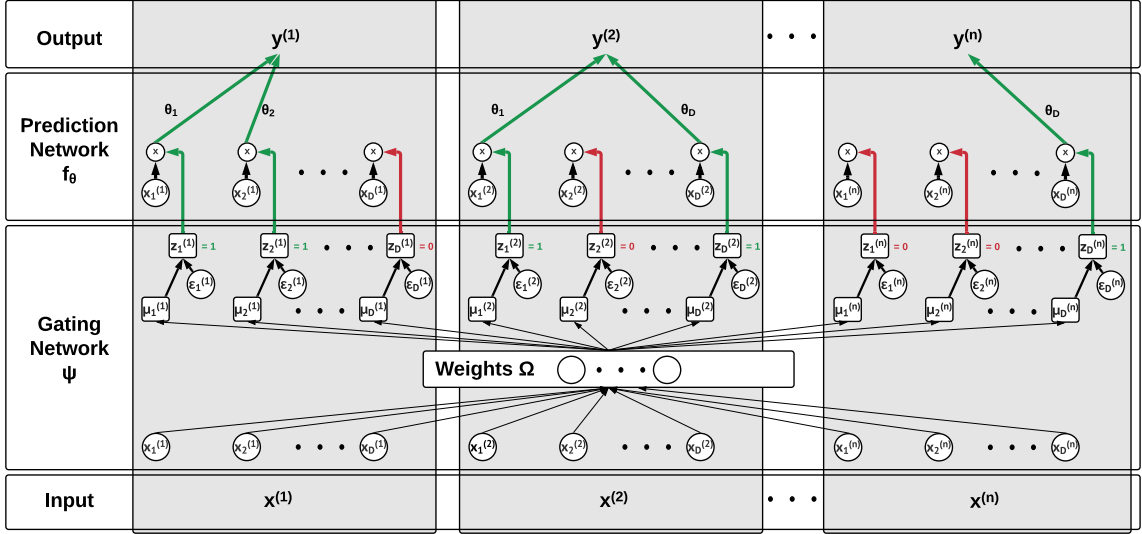


Figure 1: The architecture of Locally Linear Sparse Interpretable Networks (LLSPIN). The data $\{\mathbf{x}^{(i)} = [x_1^{(i)}, x_2^{(i)}, \dots, x_D^{(i)}]\}_{i=1}^n$ are fed simultaneously to a *gating* network Ψ and to a *prediction* network f_{θ} (which is linear in this example). The *gating* network Ψ learns to predict a set of parameters $\{\mu_d^{(i)}\}_{d=1, i=1}^{D, n}$ for each instance i in the data. The parameters $\mu_d^{(i)}$ depict the behavior of local stochastic gates $z_d^{(i)} \in [0, 1]$ that sparsify (for each instance i) the set of features that propagate into the prediction model f_{θ} . Even though the weights of the prediction networks are global, our local sparsification may lead to different prediction models for different instances. By sparsifying the number of features used for each measurement, our model can handle extreme cases of LSS, and lead to interpretable predictions (since the model only uses a small subset of features for each sample). To illustrate the behavior of LLSPIN, we overlay this figure using green (active) and red (non-active) arrows, which indicate that some samples require two features while others only one, in this example. In Section 4, we demonstrate using extensive simulations that our model, albeit its simplicity, can lead to compelling performance in the challenging regime of LSS data.

Altogether, Eq. 2 is optimized using SGD over the model parameters θ and the parameters of the *gating* network Ω . For a sample i if $\mu_d^{(i)}$ is a large number, then the d -th feature will be relevant for predicting $y^{(i)}$ with high probability (and vice versa for very small numbers).

At inference, we remove the stochasticity from the learned gates and we set $\hat{z}_d^{(i)} = \max(0, \min(1, 0.5 + \mu_d^{(i)}))$, which informs what features are selected. In practice, we observe that the values of $\hat{z}_d^{(i)}$ mostly converge to 0 or 1 (see statistics in Table 4).

Algorithm 1 Locally SParse Interpretable Networks (LSPIN) Pseudo-code

Training:

Input: observations $\{\mathbf{x}^{(i)}, y^{(i)}\}_{i=1}^N$ with $\mathbf{x}^{(i)} \in \mathbb{R}^D$, regularization parameter λ , number of epochs T , batch size B . learning rate γ

Output: Trained *gating* network Ψ_{Ω} and prediction model f_{θ}

Initialize the weights Ω of the *gating* network Ψ

for $t = 1$ **to** T **do**

for each size B batch **do**

for $i = 1$ **to** B **do**

 Compute $\boldsymbol{\mu}^{(i)} = \boldsymbol{\psi}(\mathbf{x}^{(i)}|\Omega)$

 Sample $\epsilon^{(i)}$ from $\mathcal{N}(0, \mathbf{I}\sigma^2)$, where \mathbf{I} is a $D \times D$ identity matrix

 Compute local stochastic gates $\mathbf{z}^{(i)} = \max(0, \min(1, 0.5 + \boldsymbol{\mu}^{(i)} + \epsilon^{(i)}))$

end for

 Compute the loss

$$\tilde{\mathcal{L}} = \frac{1}{B} \sum_{i=1}^B \|f_{\theta}(\mathbf{x}^{(i)} \odot \mathbf{z}^{(i)}) - y^{(i)}\|_2 + \sum_{i=1}^B \sum_{d=1}^D \left(\frac{1}{2} - \frac{1}{2} \operatorname{erf} \left(-\frac{\mu_d^{(i)} + 0.5}{\sqrt{2}\sigma} \right) \right)$$

 Update $\boldsymbol{\theta} = \boldsymbol{\theta} - \gamma \nabla_{\boldsymbol{\theta}} \tilde{\mathcal{L}}$, $\Omega = \Omega - \gamma \nabla_{\Omega} \tilde{\mathcal{L}}$

end for

end for

Inference:

Input: observations $\{\mathbf{x}^{(i)}\}_{i=1}^M$ with $\mathbf{x}^{(i)} \in \mathbb{R}^D$, Trained *gating* network Ψ_{Ω} , and prediction model f_{θ}

Output: Local gates $\{\mathbf{z}^{(i)} = \max(0, \min(1, 0.5 + \boldsymbol{\psi}(\mathbf{x}^{(i)}|\Omega))\}_{i=1}^M$

 Predictions $\{\hat{y}^{(i)} = f_{\theta}(\mathbf{x}^{(i)} \odot \mathbf{z}^{(i)})\}_{i=1}^M$

This solution is encouraged as it is stable to the injected Gaussian noise ($\epsilon_d^{(i)}$). Namely, once $\mu_d^{(i)} = -1/1$ (which are at the boundary of the range of our Tanh), the value of the corresponding $z_d^{(i)}$ would be with high probability 0 and 1, respectively. This is because the injected noise is less likely to push the values of $z_d^{(i)}$ into the range (0, 1).

3 Related Work

An extensive line of works focuses on the problem of interpretability of black box models. Methods such as [7, 8, 9] try to identify a small subset of features which explain the predictions of a pre-trained model. These models either use the gradients of the pre-trained model, or use perturbations to study the influence of different features on the predictions of each instance. However, as shown in [33] these models

either require heavy post-training computations or are inaccurate [34, 35]. More recent works such as [36, 37, 38] alleviate the computational burden by training a single model to explain all samples, but they are all designed to provide explanations of pre-trained black box models thus cannot reduce the generalization gap in case of LSS data.

Two recent works [38, 33] present solutions which allow for training a prediction model in tandem with an explanation model. However, both methods try to learn a model that “imitates” the predictions made by a baseline model which uses the full set of features. We argue, that using the full feature space in LSS data can lead to overfitting. Moreover, these methods require training a large number of parameters and use REINFORCE [28] and REBAR [30] for learning the sparsity. We demonstrate in the benchmark experiment (see Fig. 6) that the method proposed in [38] is computationally expensive and does not scale well to large datasets. We note that we attempted to compare our results to [33] but failed to run its model due to incomplete code provided.

4 Experiments

In this section, we evaluate the proposed model LLSPIN and LSPIN (linear and nonlinear versions of the model)¹, on several prediction tasks with synthetic datasets and multiple real-world datasets, where we demonstrate the interpretability of our model and compare its prediction performance with other methods including embedded methods like LASSO [21] and linear support vector classification (SVC) [39], tree-based methods like Random Forest [40] and XGBoost [41], and neural network based methods like STG [20] and INVASE [38]. Additionally we compare to RANSAC [42] for the linear synthetic example, and DeepSurv [43], COX-LASSO, COX-STG [20], and Random Survival Forest [44] for the survival analysis experiment. Details of the datasets availability, training procedure, and hyper-parameter tuning are included in the Appendix section B.

4.1 Linear Regression with Heterogeneous Clusters

In the first example, we evaluate the capabilities of the proposed model LLSPIN for a linear regression task. We generate a mixed synthetic dataset in which the response variable y of different samples depends on different subsets of features of data matrix \mathbf{X} . Specifically, \mathbf{X} has $2n$ samples and 5 features, where n i.i.d. samples (group-1) are generated from $\mathcal{N}(\mathbf{1}, 0.5\mathbf{I})$ and the other n i.i.d. samples (group-2) are generated from $\mathcal{N}(-\mathbf{1}, 0.5\mathbf{I})$ where \mathbf{I} is a 5×5 identity matrix. The corresponding response

¹Codes are available at <https://github.com/jcyang34/lspin>

variable y for samples in group-1 and group-2 is defined in Eq. 3 where for group-1, the response y is a linear combination of the 1st, 2nd, 3rd features, and for group-2 y is a linear combination of the 3rd, 4th, 5th features:

$$y = \begin{cases} -2\mathbf{x}_1 + \mathbf{x}_2 - 0.5\mathbf{x}_3, & \text{if in group-1,} \\ -0.5\mathbf{x}_3 + \mathbf{x}_4 - 2\mathbf{x}_5, & \text{otherwise.} \end{cases} \quad (3)$$

We fix the validation and test set and gradually reduce the number of training samples to compare the prediction performance of LLSPIN with 3 linear models (Linear Regression, LASSO, RANSAC) and 2 nonlinear models (Random Forest and a nonlinear fully connected Neural Network). Fig. 2a shows the performance comparison of different models where we only use 10 training samples, while results with other numbers of training samples are shown in the Appendix A. With such a limited number of training samples, linear models like Linear Regression, LASSO, and RANSAC fail to fit well because of the heterogeneous dependency on data features across the samples, whereas LLSPIN achieves accurate prediction by identifying the correct and hence interpretable features (Fig. 2b). In this example, LLSPIN (which is a linear model) outperforms nonlinear models like Random Forest and Neural Network, which further demonstrates the advantage of learning local sparsity of the features.

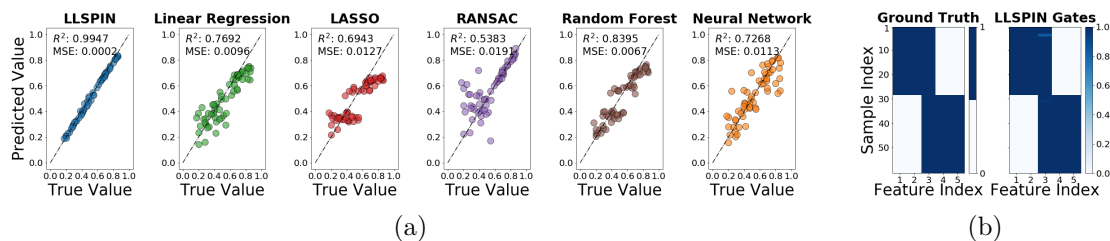


Figure 2: (a) Comparison of the model performance on unseen samples (Test set). The x-axis shows the true values y , and the y-axis shows the predicted values \hat{y} for each model. Points on the diagonal line indicate correct predictions. R-square and Mean Squared Error (MSE) are reported for each model. (b) Heat-map comparison between the ground truth explanatory features for each sample (Left, 1 for truly explanatory and 0 for not) and the identified features by LLSPIN's local gates (Right, >0 for open gates and 0 for closed). The values across the x-axis correspond to the feature indices, and the values across the y-axis correspond to the sample indices. Samples are sorted based on their ground truth group association.

4.2 Nonlinear Synthetic Datasets

In this section, we test the performance of LSPIN on synthetic data with nonlinear relations among features. First, we adapt 3 nonlinear heterogeneous synthetic datasets from [38] (**Exp 1**, **Exp 2**, and **Exp 3**) for classification, which are defined at Eq. 4, 5, and 6, separately. In each example, we generate the data matrix \mathbf{X} with 11 features sampled independently from $\mathcal{N}(\mathbf{0}, \mathbf{I})$ where \mathbf{I} is an 11×11 identity matrix. The response is $y = \mathbf{1}_A(\frac{1}{1+\text{Logit}} > 0.5)$ where $\mathbf{1}_A$ is an indicator function and the Logit for each sample is calculated based on different features depending on the sign of the 11th feature x_{11} . Additionally, to further demonstrate LSPIN’s robustness on challenging domains, we design a 4th example (termed **Exp 4** and defined in Eq. 7), for which we generate the data matrix \mathbf{X} with $2n$ samples and 4 features that consists of 2 sample groups. The first n samples are sampled from $\mathcal{N}(\mathbf{1}, 0.5\mathbf{I})$, and the second n samples are sampled from $\mathcal{N}(-\mathbf{1}, 0.5\mathbf{I})$ where \mathbf{I} is a 4×4 identity matrix. The response is defined as $y = \mathbf{1}_A(\frac{1}{1+\text{Logit}} > 0.5)$, where $\mathbf{1}_A$ is an indicator function and Logit depends on features x_1 and x_2 for the first n samples, and on features x_3 and x_4 for the remaining n samples. To make the classification task harder, we concatenate the data with 46 nuisance (irrelevant for the prediction task) features sampled from $\mathcal{N}(\mathbf{0}, 0.5\mathbf{I})$ where \mathbf{I} is an 46×46 identity matrix. We note that in all these examples we only use a limited number of samples for training as detailed in Appendix section B.

$$\mathbf{Exp\ 1:} \quad \text{Logit} = \begin{cases} \exp(\mathbf{x}_1 \times \mathbf{x}_2), & \text{if } \mathbf{x}_{11} < 0, \\ \exp(\sum_{i=3}^6 \mathbf{x}_i^2 - 4), & \text{otherwise} \end{cases} \quad (4)$$

$$\mathbf{Exp\ 2:} \quad \text{Logit} = \begin{cases} \exp(\mathbf{x}_1 \times \mathbf{x}_2), & \text{if } \mathbf{x}_{11} < 0, \\ \exp(-10 \sin(0.2\mathbf{x}_7) + |\mathbf{x}_8| + \mathbf{x}_9 + \exp(-\mathbf{x}_{10}) - 2.4), & \text{otherwise} \end{cases} \quad (5)$$

$$\mathbf{Exp\ 3:} \quad \text{Logit} = \begin{cases} \exp(\sum_{i=3}^6 \mathbf{x}_i^2 - 4), & \text{if } \mathbf{x}_{11} < 0, \\ \exp(-10 \sin(0.2\mathbf{x}_7) + |\mathbf{x}_8| + \mathbf{x}_9 + \exp(-\mathbf{x}_{10}) - 2.4), & \text{otherwise} \end{cases} \quad (6)$$

$$\mathbf{Exp\ 4:} \quad \text{Logit} = \begin{cases} \exp(\mathbf{x}_1 \times \mathbf{x}_2 - 0.9), & \text{if first } n \text{ samples} \\ \exp(\mathbf{x}_3^2 + \mathbf{x}_4^2 - 2.5), & \text{otherwise} \end{cases} \quad (7)$$

We evaluate the capabilities of LLSPIN/LSPIN and INVASE in terms of the True Positive Rate (TPR), False Discovery Rate (FDR) of the selected features. In Table 1, we compare the performance of LLSPIN/LSPIN and INVASE. In Fig. 3 we present heat-maps indicating the per sample features on the test set identified by LSPIN and

INVASE. LSPIN consistently identifies the correct features and achieves the best test accuracy. This example highlights the advantage of stochastic gating mechanism in these challenging domains.

	Exp 1					Exp 2				
	TPR (Train)	FDR (Train)	TPR (Test)	FDR (Test)	Test Accuracy	TPR (Train)	FDR (Train)	TPR (Test)	FDR (Test)	Test Accuracy
LLSPIN	0.2057	0.1596	0.2000	0.1795	0.7950	0.5544	0.0690	0.5438	0.0764	0.8900
LSPIN	0.9944	0.0060	0.9825	0.0175	0.9300	0.9827	0.0282	0.9788	0.0404	0.9550
INVASE	0.4389	0.2651	0.4438	0.2970	0.8650	0.8752	0.4169	0.8750	0.4167	0.8950
	Exp 3					Exp 4				
	TPR (Train)	FDR (Train)	TPR (Test)	FDR (Test)	Test Accuracy	TPR (Train)	FDR (Train)	TPR (Test)	FDR (Test)	Test Accuracy
LLSPIN	0.3467	0.0348	0.3480	0.0492	0.7650	0.9503	0.1554	0.9700	0.1019	0.9000
LSPIN	0.9908	0.0611	0.9850	0.0708	0.9000	0.9930	0.0493	1.0	0.0654	0.9800
INVASE	0.9002	0.4374	0.9000	0.4375	0.8500	1.0	0.4978	1.0	0.5000	0.9600

Table 1: Nonlinear synthetic classification datasets. We compare the proposed LLSPIN/LSPIN to INVASE in terms of TPR, FDR, and classification accuracy. Across these example, LSPIN correctly identifies the informative features while maintaining a substantial lower FDR and higher classification accuracy compared with INVASE.

4.3 The MNIST Dataset

In the following example we evaluate the behaviour of our linear *prediction* network (LLSPIN) on the MNIST handwritten datasets. We use 50,000 samples for training with batch size of 100 and test the model on the remaining 10,000 samples. LLSPIN attains 98.2% accuracy while selecting a small subset of pixels for each image. In Fig. 4a we present average pixel levels for the different MNIST classes. Furthermore, we superimpose the images using gates with non-zero median values (where the median is computed over all samples in each class). Here, we compare our result to REAL-X/BASE-X [33], INVASE [38], and L2X [11], and to a fully connected neural network. Results of these baseline methods were borrowed from [33]. As evident in the table presented Fig. 4b, LLSPIN leads to higher classification accuracies compared to the different baselines, while using a median amount of 7 pixels per image. This indicates that LLSPIN can learn a strong classification model while using roughly 1% of the input features for each sample.

4.4 Classification of LSS Real World Data

In this section, we evaluate LLSPIN and LSPIN on several challenging LSS real-world datasets (summarized in Table 2. BASEHOCK, RELATHE, PCMAC, COLON,

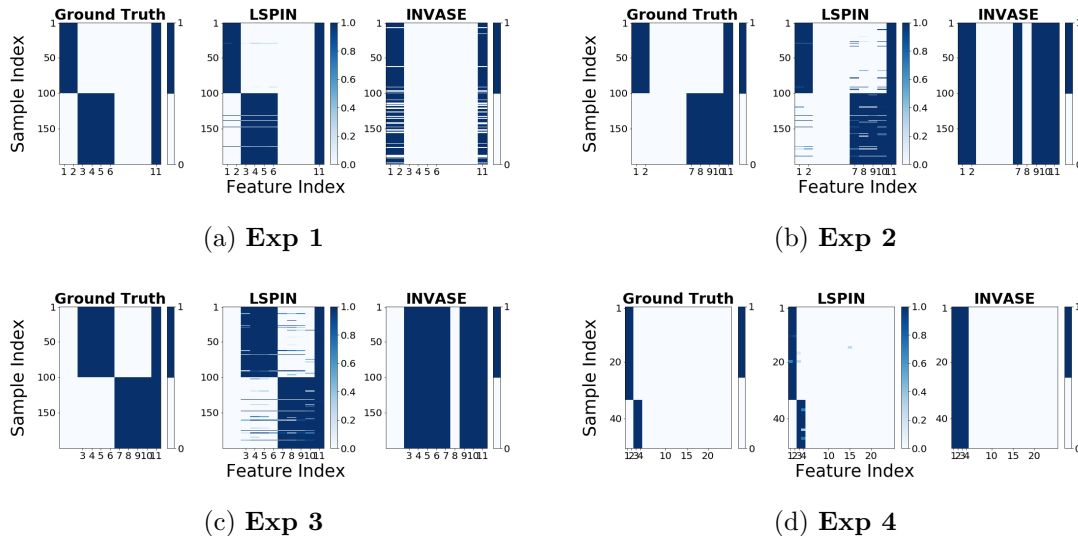


Figure 3: Informative feature identification using the synthetic classification datasets. We present heat-maps comparing the ground truth informative features (the left panel in each subfigure), and identified features by LSPIN, and INVASE based on the 4 synthetic datasets (see description in Section 4.2). For more convenient visualization we only present the first 25 features for **Exp 4**. The color indicates the activity of features, and non-zero values correspond to selected variables.

TOX171 are from the feature selection dataset collections² and the purified PBMC dataset is from [45]) and compare the performance to classification methods including LASSO, SVC, Random Forest, XGBoost, and INVASE.

	BASEHOCK	RELATHE	PCMAC	PBMC	COLON	TOX171
Number of features	4862	4322	3289	2000	2000	5748
Number of training samples	379	271	369	721	62	136
Number of test samples	1514	1084	1476	2880	13	35
Number of classes	2	2	2	4	2	4

Table 2: Properties of the real-world datasets.

Table 3 shows the comparison of the model performance on these datasets (average test accuracy and number of selected features). We can see that LLSPIN achieves state-of-the-art performance with a limited number of selected features except for the PCMAC dataset where LLSPIN uses far fewer features on average than Linear STG, to achieve similar prediction performance. This further demonstrates that for a wide

²<https://jundongli.github.io/scikit-feature/datasets.html>

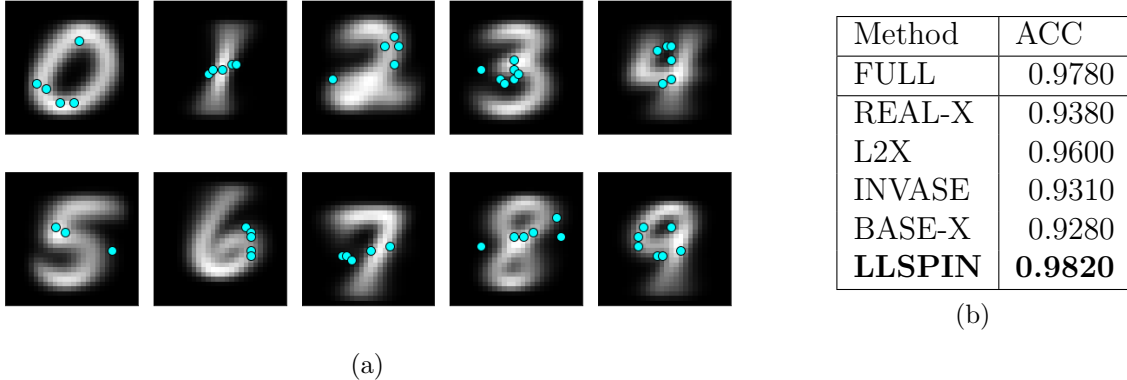


Figure 4: (a) The average pixel level per class in the MNIST dataset. For each class, we overlay the images with the median value of the gates, here the cyan dots indicate locations of non-zero gates. (b) Classification test accuracy on MNIST based on different model explanation schemes. FULL indicates accuracy of a fully connected network which uses all features. Our model outperforms REAL-X, INVASE, and BASE-X while using much fewer features per image. L2X uses less features per image, but leads to inferior classification accuracy.

range of LSS datasets, linear predictors are very effective relative to nonlinear models if features are selected individually for each instance.

	BASEHOCK	RELATHE	PCMAC	PBMC	COLON	TOX-171
LLSPIN	0.9156 ± 0.0151 [4]	0.8201 ± 0.0220 [11]	0.8148 ± 0.0174 [3]	0.9043 ± 0.0060 [18]	0.8385 ± 0.0538 [7]	0.9257 ± 0.0641 [6]
LSPIN	0.8937 ± 0.0148 [3]	0.8059 ± 0.0195 [3]	0.7851 ± 0.0148 [3]	0.8867 ± 0.0064 [15]	0.7154 ± 0.0692 [1]	0.9029 ± 0.0545[1]
Linear STG	0.8936 ± 0.0140 [27]	0.6994 ± 0.0505 [16]	0.8511 ± 0.0107 [42]	0.8822 ± 0.0082 [27]	0.7462 ± 0.1144 [14]	0.7114 ± 0.0578 [16]
Nonlinear STG	0.8924 ± 0.0118 [20]	0.7483 ± 0.0395 [27]	0.8416 ± 0.0090 [32]	0.8629 ± 0.0131 [19]	0.7615 ± 0.1395 [8]	0.6743 ± 0.0725 [14]
INVASE	0.8402 ± 0.0081 [42]	0.7081 ± 0.0156 [43]	0.7706 ± 0.0101 [48]	0.8634 ± 0.0081 [30]	0.7692 ± 0.1240 [6]	0.7686 ± 0.0739[26]
LASSO	0.7446 ± 0.0519 [34]	0.5869 ± 0.0159 [18]	0.6809 ± 0.0408 [21]	0.9030 ± 0.0036 [31]	0.8154 ± 0.0985 [24]	0.8771 ± 0.0462 [49]
XGBoost	0.9037 ± 0.0105 [45]	0.7675 ± 0.0167 [32]	0.8393 ± 0.0067 [43]	0.7658 ± 0.0072 [64]	0.7615 ± 0.1214 [7]	0.6743 ± 0.0560 [38]
SVC	0.7446 ± 0.0337 [22]	0.5648 ± 0.0300 [6]	0.6741 ± 0.0372 [12]	0.8902 ± 0.0074 [30]	0.7615 ± 0.0939 [25]	0.8114 ± 0.0747 [38]
Random Forest	0.6446 ± 0.0452 [10]	0.7142 ± 0.0350 [50]	0.6744 ± 0.0700 [9]	0.4856 ± 0.0618 [10]	0.7923 ± 0.0976 [47]	0.5371 ± 0.0996 [42]
NN (all features)	0.5651 ± 0.0143	0.5544 ± 0.0238	0.5438 ± 0.0127	0.6157 ± 0.0145	0.8154 ± 0.0784	0.6259 ± 0.0803

Table 3: Comparing the classification accuracy on real-world datasets using different prediction models. For each method the average accuracy and standard deviation are reported, with the corresponding average number of selected features in the square brackets. NN refers to a fully connected network trained based on the complete feature set.

4.5 Cox Proportional Hazard Models for Survival Analysis

In Survival Analysis, instance-level interpretation of the selected features is of particular interest as it can identify what are the top predictive features among a heterogeneous

population. Here we combine our models (LSPIN/LLSPIN) with DeepSurv [43] which is a neural network framework for Cox model, and apply the integrated models (COX-LLSPIN/COX-LSPIN) on a Surveillance, Epidemiology, and End Results (SEER) breast cancer dataset [46] to perform survival analysis.

We compare the performance (Test Concordance Index (C-Index) w.r.t. the number of selected features) with other Survival Analysis models (DeepSurv, COX-LASSO, COX-STG (Linear/Nonlinear), and Random Survival Forest) as shown in Fig. 5a. We can see that the COX-LLSPIN/COX-LSPIN models achieve the best performance when limiting the number of active features. Furthermore, the performance is comparable to the state-of-the-art models which are trained on all features.

Fig. 5b shows the frequency of the selected feature sets among samples from one training case of COX-LLSPIN. For instance, 57.2% of the samples have “Age” and “TsizeMerged” features selected as factors that are important for the prediction, while 1.2% of the samples have only “NodesRatio” feature selected, which demonstrates that the heterogeneity among these samples can be characterized by COX-LLSPIN/COX-LSPIN models.

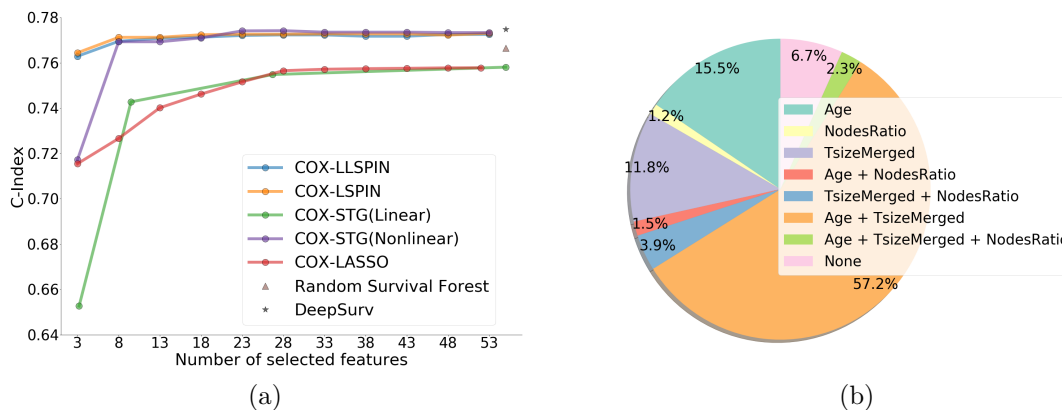


Figure 5: Survival Analysis on the SEER breast cancer data. (a) Comparing the test Concordance Index (C-Index) of several baselines on the SEER data. (b) Frequency of feature sets used by LLSPIN for prediction across the different patients.

4.6 Running Time Benchmark

To demonstrate the computational efficiency of our models, we compare the training running time between LLSPIN/LSPIN and INVASE on the nonlinear synthetic example **Exp 1** (Eq. 4) where we vary the number of training samples (200, 600, 1000, 1400, 1800)

as shown in Fig. 6. We can see that the running time of INVASE increases rapidly with more training samples whereas our models remain scalable.

To perform a fair comparison, we design the architecture of LLSPIN/LSPIN/INVASE using 2 hidden layers with 200 neurons each, and we set 2 hidden layers with 100 neurons each for the *gating* network of LLSPIN/LSPIN and the selector network of INVASE. For all the 3 models, λ is set to 1, batch size is set to full batch training, and epochs is set to 3000. We set the learning rate for INVASE to 0.0001 (Adam optimizer), and 0.1 for SGD optimizer of LLSPIN/LSPIN.

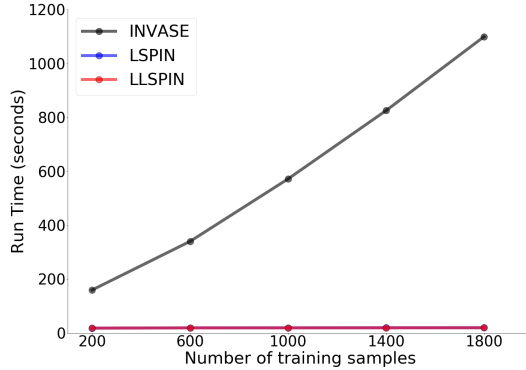


Figure 6: Time Benchmark between LLSPIN/LSPIN and INVASE. The proposed model is more scalable to large datasets.

5 Conclusion

In this study, we present a method for learning locally sparse neural networks. For each observation our model predicts the target based on a small subset of variables. This leads to an interpretable model, which can handle cases of low-sample-size (LSS) data that is either high dimensional, or contains nuisance features. We predict the subset of informative features using a *gating* network which we train simultaneously with a *prediction* network. We demonstrate using synthetic and real datasets, that our model can outperform state-of-the-art classification and regression models. Furthermore, when applied to datasets with nuisance variables, our model correctly identifies the subsets of informative features.

Acknowledgements

The authors thank Mihir Khunte and Michal Marczyk for the preprocessing steps of the SEER breast cancer data.

References

- [1] Naftali Tishby and Noga Zaslavsky. Deep learning and the information bottleneck principle. In *2015 IEEE Information Theory Workshop (ITW)*, pages 1–5. IEEE, 2015.
- [2] Raman Arora, Amitabh Basu, Poorya Mianjy, and Anirbit Mukherjee. Understanding deep neural networks with rectified linear units. *arXiv preprint arXiv:1611.01491*, 2016.
- [3] Atsushi Yaguchi, Taiji Suzuki, Wataru Asano, Shuhei Nitta, Yukinobu Sakata, and Akiyuki Tanizawa. Adam induces implicit weight sparsity in rectifier neural networks. In *2018 17th IEEE International Conference on Machine Learning and Applications (ICMLA)*, pages 318–325. IEEE, 2018.
- [4] Daniel Soudry, Elad Hoffer, Mor Shpigel Nacson, Suriya Gunasekar, and Nathan Srebro. The implicit bias of gradient descent on separable data. *The Journal of Machine Learning Research*, 19(1):2822–2878, 2018.
- [5] Bo Liu, Ying Wei, Yu Zhang, and Qiang Yang. Deep neural networks for high dimension, low sample size data. In *IJCAI*, pages 2287–2293, 2017.
- [6] Makoto Aoshima, Dan Shen, Haipeng Shen, Kazuyoshi Yata, Yi-Hui Zhou, and JS Marron. A survey of high dimension low sample size asymptotics. *Australian & New Zealand journal of statistics*, 60(1):4–19, 2018.
- [7] Karen Simonyan, Andrea Vedaldi, and Andrew Zisserman. Deep inside convolutional networks: Visualising image classification models and saliency maps. *arXiv preprint arXiv:1312.6034*, 2013.
- [8] Matthew D Zeiler and Rob Fergus. Visualizing and understanding convolutional networks. In *European conference on computer vision*, pages 818–833. Springer, 2014.
- [9] Scott Lundberg and Su-In Lee. A unified approach to interpreting model predictions. *arXiv preprint arXiv:1705.07874*, 2017.
- [10] Marco Tulio Ribeiro, Sameer Singh, and Carlos Guestrin. " why should i trust you?" explaining the predictions of any classifier. In *Proceedings of the 22nd ACM SIGKDD international conference on knowledge discovery and data mining*, pages 1135–1144, 2016.

- [11] Jianbo Chen, Le Song, Martin Wainwright, and Michael Jordan. Learning to explain: An information-theoretic perspective on model interpretation. In *International Conference on Machine Learning*, pages 883–892. PMLR, 2018.
- [12] Peter Hall, James Stephen Marron, and Amnon Neeman. Geometric representation of high dimension, low sample size data. *Journal of the Royal Statistical Society: Series B (Statistical Methodology)*, 67(3):427–444, 2005.
- [13] Sungkyu Jung, J Stephen Marron, et al. Pca consistency in high dimension, low sample size context. *The Annals of Statistics*, 37(6B):4104–4130, 2009.
- [14] Kazuyoshi Yata and Makoto Aoshima. Effective pca for high-dimension, low-sample-size data with noise reduction via geometric representations. *Journal of multivariate analysis*, 105(1):193–215, 2012.
- [15] Lingsong Zhang and Xihong Lin. Some considerations of classification for high dimension low-sample size data. *Statistical methods in medical research*, 22(5):537–550, 2013.
- [16] Liran Shen, Meng Joo Er, and Qingbo Yin. The classification for high-dimension low-sample size data. *arXiv preprint arXiv:2006.13018*, 2020.
- [17] Yifeng Li, Chih-Yu Chen, and Wyeth W Wasserman. Deep feature selection: theory and application to identify enhancers and promoters. *Journal of Computational Biology*, 23(5):322–336, 2016.
- [18] Simone Scardapane, Danilo Comminiello, Amir Hussain, and Aurelio Uncini. Group sparse regularization for deep neural networks. *Neurocomput.*, 241(C):81–89, June 2017.
- [19] J. Feng and N. Simon. Sparse-Input Neural Networks for High-dimensional Nonparametric Regression and Classification. *ArXiv e-prints*, November 2017.
- [20] Yutaro Yamada, Ofir Lindenbaum, Sahand Negahban, and Yuval Kluger. Feature selection using stochastic gates. In *International Conference on Machine Learning*, pages 10648–10659. PMLR, 2020.
- [21] Robert Tibshirani. Regression shrinkage and selection via the lasso. *Journal of the Royal Statistical Society. Series B (Methodological)*, pages 267–288, 1996.
- [22] Jianqing Fan and Runze Li. Variable selection via nonconcave penalized likelihood and its oracle properties. *Journal of the American statistical Association*, 96(456):1348–1360, 2001.

- [23] Ofir Lindenbaum and Stefan Steinerberger. Randomly aggregated least squares for support recovery. *Signal Processing*, 180:107858, 2021.
- [24] Ofir Lindenbaum and Stefan Steinerberger. Refined least squares for support recovery. *arXiv preprint arXiv:2103.10949*, 2021.
- [25] Christos Louizos, Max Welling, and Diederik P. Kingma. Learning sparse neural networks through l0 regularization. *CoRR*, abs/1712.01312, 2017.
- [26] Eric Jang, Shixiang Gu, and Ben Poole. Categorical reparameterization with gumbel-softmax. *arXiv preprint arXiv:1611.01144*, 2016.
- [27] Ofir Lindenbaum, Moshe Salhov, Amir Averbuch, and Yuval Kluger. ℓ_0 -based sparse canonical correlation analysis. *arXiv preprint arXiv:2010.05620*, 2020.
- [28] Ronald J. Williams. Simple statistical gradient-following algorithms for connectionist reinforcement learning. *Machine Learning*, 8:229–256, 1992.
- [29] Yoshua Bengio, Aaron Courville, and Pascal Vincent. Representation learning: A review and new perspectives. *IEEE transactions on pattern analysis and machine intelligence*, 35(8):1798–1828, 2013.
- [30] George Tucker, Andriy Mnih, Chris J Maddison, Dieterich Lawson, and Jascha Sohl-Dickstein. Rebar: Low-variance, unbiased gradient estimates for discrete latent variable models. *arXiv preprint arXiv:1703.07370*, 2017.
- [31] Chris J Maddison, Andriy Mnih, and Yee Whye Teh. The concrete distribution: A continuous relaxation of discrete random variables. *arXiv preprint arXiv:1611.00712*, 2016.
- [32] Christos Louizos, Max Welling, and Diederik P Kingma. Learning sparse neural networks through l_0 regularization. *arXiv preprint arXiv:1712.01312*, 2017.
- [33] Neil Jethani, Mukund Sudarshan, Yindalon Aphinyanaphongs, and Rajesh Ranganath. Have we learned to explain?: How interpretability methods can learn to encode predictions in their interpretations. In *International Conference on Artificial Intelligence and Statistics*, pages 1459–1467. PMLR, 2021.
- [34] Julius Adebayo, Justin Gilmer, Michael Muelly, Ian Goodfellow, Moritz Hardt, and Been Kim. Sanity checks for saliency maps. *arXiv preprint arXiv:1810.03292*, 2018.
- [35] Trevor Gale, Erich Elsen, and Sara Hooker. The state of sparsity in deep neural networks. *arXiv preprint arXiv:1902.09574*, 2019.

- [36] Piotr Dabkowski and Yarin Gal. Real time image saliency for black box classifiers. *arXiv preprint arXiv:1705.07857*, 2017.
- [37] Patrick Schwab and Walter Karlen. Cxplain: Causal explanations for model interpretation under uncertainty. *arXiv preprint arXiv:1910.12336*, 2019.
- [38] Jinsung Yoon, James Jordon, and Mihaela van der Schaar. Invase: Instance-wise variable selection using neural networks. In *International Conference on Learning Representations*, 2018.
- [39] Yin-Wen Chang and Chih-Jen Lin. Feature ranking using linear svm. In *Causation and Prediction Challenge*, pages 53–64, 2008.
- [40] Ramón Díaz-Uriarte and Sara Alvarez De Andres. Gene selection and classification of microarray data using random forest. *BMC bioinformatics*, 7(1):3, 2006.
- [41] Tianqi Chen and Carlos Guestrin. Xgboost: A scalable tree boosting system. In *Proceedings of the 22nd acm sigkdd international conference on knowledge discovery and data mining*, pages 785–794. ACM, 2016.
- [42] Martin A Fischler and Robert C Bolles. Random sample consensus: a paradigm for model fitting with applications to image analysis and automated cartography. *Communications of the ACM*, 24(6):381–395, 1981.
- [43] Jared L. Katzman, Uri Shaham, Alexander Cloninger, Jonathan Bates, Tingting Jiang, and Yuval Kluger. Deepsurv: personalized treatment recommender system using a cox proportional hazards deep neural network. *BMC Medical Research Methodology*, 18, 2018.
- [44] Hemant Ishwaran, Udaya B. Kogalur, Eugene H. Blackstone, and Michael S. Lauer. Random survival forests. *Annals of Applied Statistics*, 2(3):841–860, 9 2008.
- [45] Grace XY Zheng, Jessica M Terry, Phillip Belgrader, Paul Ryvkin, Zachary W Bent, Ryan Wilson, Solongo B Ziraldo, Tobias D Wheeler, Geoff P McDermott, Junjie Zhu, et al. Massively parallel digital transcriptional profiling of single cells. *Nature communications*, 8:14049, 2017.
- [46] Surveillance, epidemiology, and end results (SEER) program research data (1975–2016). In National Cancer Institute, DCCPS, Surveillance Research Program, Surveillance Systems Branch, released April 2019, based on the November 2018 submission. SEER. (www.seer.cancer.gov).

- [47] Xavier Glorot and Yoshua Bengio. Understanding the difficulty of training deep feedforward neural networks. In *Proceedings of the thirteenth international conference on artificial intelligence and statistics*, pages 249–256, 2010.
- [48] Takuya Akiba, Shotaro Sano, Toshihiko Yanase, Takeru Ohta, and Masanori Koyama. Optuna: A next-generation hyperparameter optimization framework. *KDD*, 2019.

Appendix

A Additional Results

In the following section, we provide additional experimental results to support the effectiveness of the proposed approach.

A.1 Linear Synthetic Dataset

First, we extend our evaluation from our main text using the linear synthetic dataset (see description in Section 4.1) with different number of training samples (60,30,18,12,6). Fig. 7a demonstrates that LLSPIN consistently outperforms all other methods. Fig. 7b reveals that in each case, LLSPIN correctly uncovers the corresponding interpretable features for each sample in the gate matrices compared to the ground truth, except when the training is limited with just 6 training samples where LLSPIN misses one feature for the second sample group. This simulation demonstrates the effectiveness of LLSPIN on low sample size (LSS) datasets.

A.2 Nonlinear Synthetic Datasets

In the following subsection, we demonstrate LSPIN’s interpretability capabilities. We examine the sparsification patterns of LSPIN (along with INVASE and ground truth informative features) on the training sets for the 4 nonlinear synthetic examples (see Section 4.2 for details). As shown in Fig. 8 LSPIN correctly identifies the informative features in these four examples.

A.3 Sparsity of the Local Gates

To demonstrate that our model performs local sparsification of input features, we evaluate the statistics of the converged gate values. Table 4 presents the distribution of local gates’ values in the linear/nonlinear synthetic experiments. Our results demonstrate that most gates converge to 0 and 1 with only a few gates converge to values in the range (0, 1).

A.4 Time Benchmark Additional Result

Here, we provide a complementary time benchmark experiment (Fig. 9) to the result presented in the main text (see Fig. 6 from Section 4.6). We use the dataset from **Exp 2** (See description in Section 4.2) and generate additional noisy features (2000 features in total including the informative 11 features) by sampling values from $\mathcal{N}(0, 1)$. In this

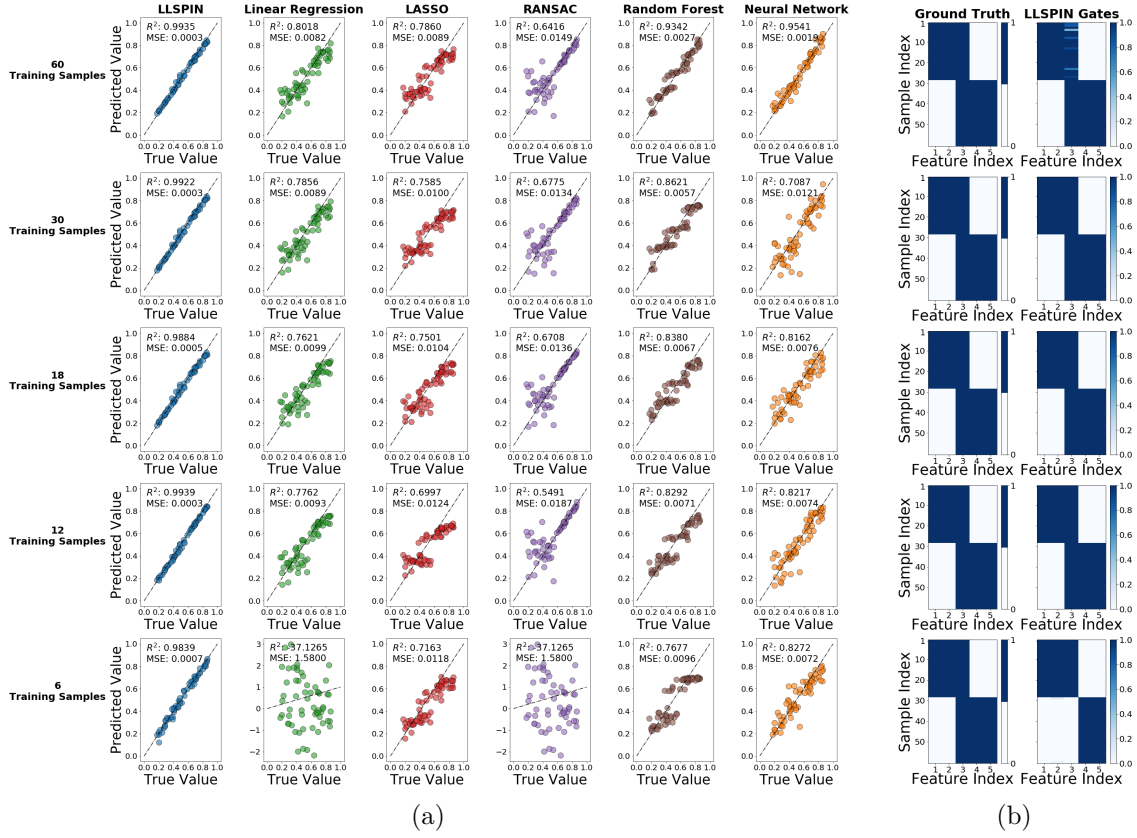


Figure 7: (a) Evaluation of the performance for different training sizes. Each row indicates a different number of training samples, from top to bottom: 60, 30, 18, 12, and 6, respectively. The x-axis represents the true target value y , and the y-axis presents the predicted value \hat{y} for each model (as indicated in the subtitles of the columns). Points on the diagonal line indicate correct predictions. R-square and Mean Squared Error (MSE) are reported for each model. (b) Heat-map comparison between the ground truth informative features for each sample (Left, 1 for truly informative and 0 for not) and the identified features by LLSPIN’s local gates (Right, >0 for open gates and 0 for closed gates). The values across the x-axis correspond to the feature indices, and the values across the y-axis correspond to the sample indices. Samples are sorted based on their group association (see model description in Eq. 3).

high dimensional regime, LLSPIN/LSPIN remains scalable compared with INVASE. For LLSPIN/LSPIN/INVASE we use the same architectures and parameter settings as in Section 4.6.

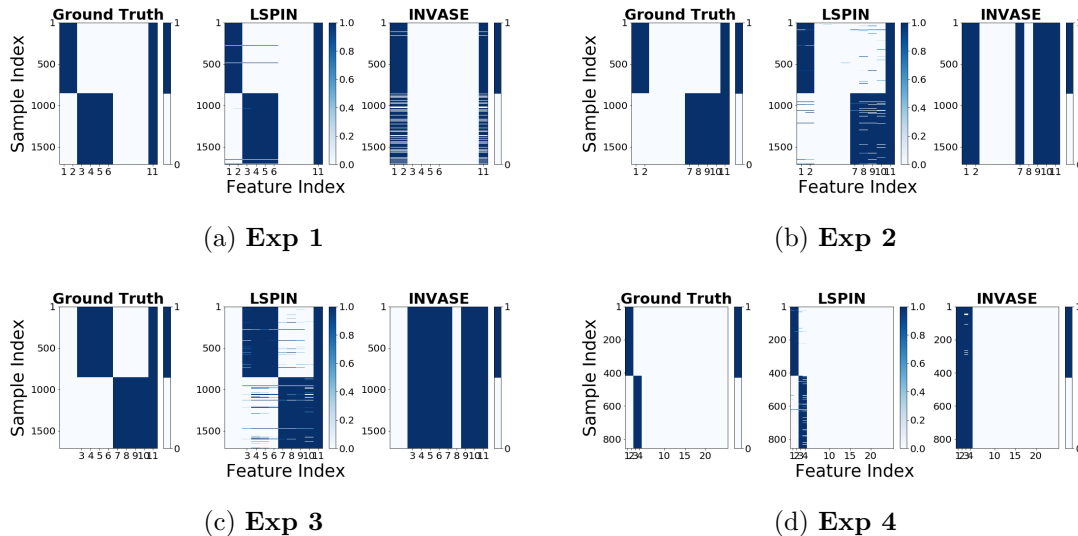


Figure 8: Feature subset identification using the synthetic classification datasets. We present heat-maps comparing the ground truth informative features (left panel in each subfigure) with the identified features by LSPIN and INVASE based on the 4 synthetic datasets. For ease of visualization we only present the leading 25 features for **Exp 4**. The color indicates the activity of features, and non-zero values correspond to selected variables.

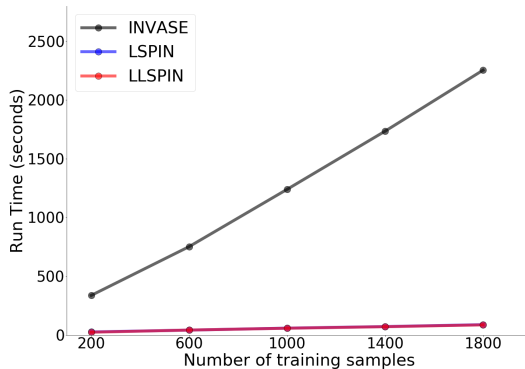


Figure 9: Time benchmark experiment between INVASE and LLSPIN/LSPIN

B Reproducibility and Additional Details

In the following subsections, we provide additional experimental details required for the reproduction of the experiments provided in the main text. All the experiments are conducted using Intel(R) Xeon(R) Gold 6150 CPU @ 2.70GHz (72 cores total).

Experiments	Models	Training			Test		
		% of 0s	% of 1s	% 0-1	% of 0s	% of 1s	% 0-1
Linear 60 samples	LLSPIN	40.00	57.67	2.33	40.00	57.33	2.67
Linear 30 samples	LLSPIN	40.00	60.00	0.00	40.00	60.00	0.00
Linear 18 samples	LLSPIN	40.00	60.00	0.00	40.00	60.00	0.00
Linear 12 samples	LLSPIN	40.00	60.00	0.00	40.00	60.00	0.00
Linear 10 samples	LLSPIN	40.00	58.00	2.00	40.00	59.33	0.67
Linear 6 samples	LLSPIN	50.00	50.00	0.00	50.00	49.33	0.67
Nonlinear Exp 1	LLSPIN	91.11	8.60	0.29	91.14	7.27	1.59
	LSPIN	63.64	36.27	0.09	63.64	35.95	0.41
Nonlinear Exp 2	LLSPIN	78.36	20.68	0.96	78.59	20.09	1.32
	LSPIN	63.25	35.53	1.22	62.91	35.59	1.50
Nonlinear Exp 3	LLSPIN	83.67	13.69	2.63	83.36	13.32	3.32
	LSPIN	52.04	44.90	3.07	51.82	44.73	3.45
Nonlinear Exp 4	LLSPIN	95.50	3.56	0.94	95.68	3.28	1.04
	LSPIN	95.82	3.74	0.44	95.72	3.68	0.60

Table 4: Statistics of the local gate values. The percentage of gates between 0 and 1 is listed in bold.

We apply batch normalization to the *prediction* network of LLSPIN/LSPIN and STG models throughout the experiments, except for the MNIST and survival analysis experiments. We note that application of batch normalization in the MNIST experiment did not improve performance. In the survival analysis, the performance was satisfactory without application of batch normalization.

For LLSPIN/LSPIN/STG models, the network weights are initialized by drawing from $\mathcal{N}(0, s)$. For LLSPIN/LSPIN, we set s to be 0.1 for the synthetic datasets experiments, MNIST example, and time benchmark experiments. We set $s = \frac{1}{\sqrt{D}}$ (D is the input dimensionality) following Xavier initialization [47] for the real-world examples, and $s = 0.05$ for the cox survival analysis. For STG models, s is set to 0.1 for the real-world datasets and 0.05 for the cox survival analysis. For all the experiments, we use tanh as the hidden layer activation function for both the *gating* network of LLSPIN/LSPIN and the nonlinear *prediction* network of LSPIN/STG. For INVASE, we use relu activation as suggested in [38].

B.1 Regularization Term

Our regularizer is expressed by:

$$\begin{aligned}
 \mathbb{E}_Z \|\mathbf{Z}\|_0 &= \sum_{d=1}^D \mathbb{P}[z_d > 0] = \sum_{d=1}^D \mathbb{P}[\mu_d + \sigma\epsilon_d + 0.5 > 0] \\
 &= \sum_{d=1}^D \{1 - \mathbb{P}[\mu_d + \sigma\epsilon_d + 0.5 \leq 0]\} \\
 &= \sum_{d=1}^D \left\{1 - \Phi\left(\frac{-\mu_d - 0.5}{\sigma}\right)\right\} \\
 &= \sum_{d=1}^D \Phi\left(\frac{\mu_d + 0.5}{\sigma}\right) \\
 &= \sum_{d=1}^D \left(\frac{1}{2} - \frac{1}{2} \operatorname{erf}\left(-\frac{\mu_d + 0.5}{\sqrt{2}\sigma}\right)\right)
 \end{aligned}$$

To tune σ , we follow the suggestion in [20]. Specifically, the effect of σ can be understood by looking at the value of $\frac{\partial}{\partial \mu_d} \mathbb{E}_Z \|\mathbf{Z}\|_0$. In the first training step, μ_d is 0. Therefore, at initial training phase, $\frac{\partial}{\partial \mu_d} \mathbb{E}_Z \|\mathbf{Z}\|_0$ is close to $\frac{1}{\sqrt{2\pi\sigma^2}} e^{-\frac{1}{8\sigma^2}}$. To enable sparsification, this term (multiplied by the regularization parameter λ) has to be greater than the derivative of the loss with respect to μ_d because otherwise μ_d is updated in the incorrect direction. To encourage such behavior, we tune σ to the value that maximizes the gradient of the regularization term. As demonstrated in Fig. 10 this is obtained when $\sigma = 0.5$. Therefore, we keep $\sigma = 0.5$ throughout our experiments.

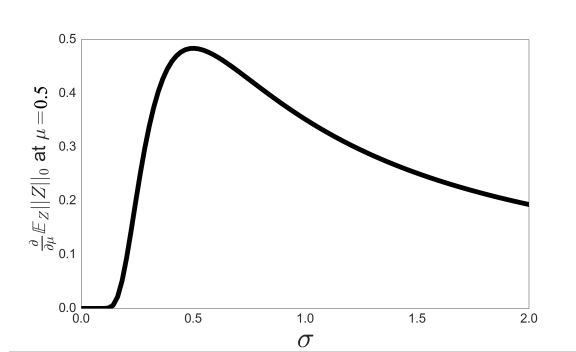


Figure 10: The value of $\frac{\partial}{\partial \mu} \mathbb{E}_Z \|\mathbf{Z}\|_0|_{\mu=0.5} = \frac{1}{\sqrt{2\pi\sigma^2}} e^{-\frac{1}{8\sigma^2}}$ for $\sigma = [0.001, 2]$.

B.2 Linear Regression Example Details

Here we provide details for reproduction of the example presented in Section 4.1.

B.2.1 Data Generation and Split

The data matrix \mathbf{X} contains $2n = 600$ samples where the first 300 samples (group-1) are i.i.d. based on $\mathcal{N}(\mathbf{1}, 0.5\mathbf{I})$, and the remaining 300 i.i.d. samples (group-2) are drawn from $\mathcal{N}(-\mathbf{1}, 0.5\mathbf{I})$ where \mathbf{I} is a 5×5 identity matrix. We randomly select 60 samples as validation set, 60 samples as the test set, and we randomly select subsets of size 60,30,18,12,10,6 samples as our training sets.

B.2.2 Training Procedures and Hyper-parameter Tuning and Settings

For LLSPIN, LASSO, Random Forest, Neural Network, we optimize each model using 100 trials of Optuna (a hyper-parameter optimization software [48]) on the validation set, with parameter ranges listed in Table 5. After Optuna selects the parameters, we test each model’s performance on the test set. INVASE was not included in this comparison because in its current implementation it is not applicable for regression tasks.

Parameters	Search Range
learning rate (LLSPIN,Neural Net)	[1e-2,2e-1]
epochs (LLSPIN,Neural Net)	{2000, 5000, 10000, 15000}
λ (LLSPIN)	[1e-3,1e-2]
α (LASSO)	[1e-3,5e-1]
n_estimators (RF)	[1,500]
max_depth (RF)	[1,30]
min_samples_split (RF)	[2,10]

Table 5: Parameter search ranges for the linear synthetic example.

In this example, we use 4 hidden layers with 100, 100, 10, 1 neurons in each layer respectively. For the *gating* network we use 1 hidden layer with 10 neurons. We use full batch training.

B.3 Nonlinear Synthetic Datasets Details

Here we provide details for reproduction of the example presented in Section 4.2.

B.3.1 Data Generation and Split

Exp 1, Exp 2, Exp 3 are adapted from [38], where we generate 2000 samples with 11 features for each experiment (see Section 4.2 for a description of these datasets). To evaluate a LSS regime, the number of samples we use is far fewer compared with the number of samples used in experiments conducted in [38]. We split the data and use 90% for training and 10% for testing. 5% of the training set is set aside as validation set. For **Exp 4**, we generate $2n = 1000$ samples and we split the data and use 95% for training and 5% for testing. 10% of the training set is set aside as validation set.

B.3.2 Training Procedures and Hyper-parameter Tuning and Settings

For these synthetic 4 experiments, we optimize each model on the validation set using Optuna with grids of parameters listed in Table 6, then we evaluate the models on the unseen test sets.

The number of hidden layers and nodes are identical for LLSPIN, LSPIN, and INVASE. For **Exp 2, Exp 3, Exp 4**, we use 2 hidden layers with 200 nodes each for the *prediction* network architecture. We use 2 layers with 100 nodes each for the *gating* network of LLSPIN/LSPIN and the selector network of INVASE. For **Exp 1**, we add one layer with 200 nodes to the *prediction* network architecture for all models, and one layer with 100 nodes to the *gating* network of LLSPIN/LSPIN and selector network of INVASE.

	Batch Size	Number of Epochs	Learning Rate	λ
Exp 1	Full	10000	1e-1 (LLSPIN/LSPIN) 1e-4 (INVASE)	[2e-1,3e-1]
Exp 2	Full	10000	1e-1 (LLSPIN/LSPIN) 1e-4 (INVASE)	[0.15,0.2]
Exp 3	Full	3000	1e-1 (LLSPIN/LSPIN) 1e-4 (INVASE)	[0.15,0.2]
Exp 4	Full	{1000, 1200}	[3e-2,5e-2] (LLSPIN/LSPIN) [1e-5,1e-4] (INVASE)	[1.33,1.35]

Table 6: Parameter search ranges for the 4 nonlinear experiments. We run 5 Optuna trials on the grids of λ for **Exp 1, Exp 2, Exp 3** and 20 trials on the grids of epochs, learning rate, λ for **Exp 4**. For INVASE we use Adam Optimizer while other baselines are based on standard SGD.

B.4 Real-world Datasets Details

Here we provide details for reproduction of the example presented in Section 4.4.

B.4.1 PBMC Dataset Preprocessing Steps

The purified Peripheral Blood Mononuclear Cells (PBMC) dataset was collected by [45], in which the data represents individual cells with gene values. Each entry represents the the number of mRNAs expressed by a gene within a cell. This data matrix is first filtered (cells that have less than 400 expressed genes are excluded, and genes that are expressed in less than 100 cells are excluded) and normalized by the library size (total number of mRNAs expressed per cell). We then exclude the non protein-coding genes, and retain only cells that belong to the following 4 cell types: memory T cells, naive T cells, regulatory T cells, naive cytotoxic T cells.

We use 34,115 cells (90% of the data) to select the 2000 most variable genes and use the remaining 3,791 cells (10% of the data) with these 2000 genes as the final processed dataset to further split training/test/validation sets as described in the next subsection.

B.4.2 Training Procedures

In this section, we introduce our training procedures for the real-world LSS datasets. Specifically, for the BASEHOCK, RELATHE, PCMAC, and PBMC datasets, 5% of each dataset is set aside as validation set. Let us denote the remaining 95% of the data as $\bar{\mathbf{X}}$. We then split $\bar{\mathbf{X}}$ into 5 non-overlapping folds.

We train each model on the 1st fold of $\bar{\mathbf{X}}$ and test it on the remaining non-overlapping 4 folds. The hyper-parameters are optimized on the validation set via Optuna (50 trials for the neural network-based methods and tree-based methods and 5 trials for INVASE due to long computation time) trained on the 1st fold of $\bar{\mathbf{X}}$. These (fixed) hyper-parameters are then used in training the model on the second fold and testing it on the remaining 4 non-overlapping folds. Similarly, we use these fixed hyper-parameters to train models for folds No.3, No.4 and No.5, and each time test these models on the remaining 4 non-overlapping folds. This training and testing procedure is repeated for several regularization parameters, then we report the best average performance for each method.

Since COLON and TOX-171 are of extreme LSS, we simply use a grid of regularization parameters for each method and identify the best average performance (test accuracy and number of selected features) across 10 runs (using 80% of the samples for training and 20% for testing).

The regularization parameters are tuned to select fewer than 50 features, except for XGBoost with the PBMC dataset which produced a minimum number of feature

selected of 64. For local methods including LLSPIN, LSPIN, and INVASE, the average (over the 5 folds) median (over the samples) number of selected features is reported.

B.4.3 Hyper-parameter Tuning and Settings

For LLSPIN/LSPIN/STG/Neural Network model, the *prediction* network architecture is set to 3 hidden layers with 100, 50, 30 neurons respectively for all the datasets. The *gating* network for LLSPIN/LSPIN models is set to one single layer with 500 neurons for BASEHOCK, RELATHE, PCMAC, PBMC datasets, and 2 hidden layers with 100 and 10 neurons respectively for the COLON and TOX-171 datasets. For INVASE, the predictor network has 2 hidden layers and 200 neurons on each layer, and the selector network has 2 hidden layers and 100 neurons on each layer (as suggested by the authors).

The search range for the regularization parameter λ are listed in Table 7, along with the grids of learning rate and epochs that are optimized via Optuna for the BASEHOCK, RELATHE, PCMAC, PBMC datasets, and the settings of learning rate and epochs in the COLON and TOX-171 datasets. We use full batch training for all neural network based methods for all 6 datasets.

In the TOX-171 dataset, we have increased the search range of λ values to $[1,10]$ to enable effective sparsification of the feature space. For LASSO and SVC, the search range for c is $[1e-3,1e-1]$ for BASEHOCK, RELATHE, PCMAC, PBMC datasets, and $[1e-2,1e3]$ for COLON and TOX-171 datasets.

For Random Forest and XGBoost, we use `number_of_estimators` to replace the regularization parameter proposed in the previously training procedures. The grid of `number_of_estimators` is $\{1,5,10,20,30,50,100,200,500,1000\}$ for both methods when we applied them to the BASEHOCK, RELATHE, PCMAC, PBMC datasets, and is $\{1,2,3,4,5,8,10,15,20,25,30,40,50,60,70,80,100,200,500,1000\}$ when we applied them to the COLON and TOX-171 datasets.

Other parameter settings for XGBoost are as follows: For the BASEHOCK, RELATHE, PCMAC, PBMC datasets, we optimize `max_depth` via Optuna with grid range $[1,10]$. For the COLON and TOX-171 datasets, we set `max_depth` to 10.

Other parameter settings for Random Forest are as follows: For the BASEHOCK, RELATHE, PCMAC, PBMC datasets, we optimize `max_depth` and `minimum_samples_to_split` via Optuna with grid range $[1,10]$ and $[2,50]$, respectively. For the COLON and TOX-171 datasets, we set `max_depth` to 10 and `minimum_samples_to_split` to 5.

Dataset	Method	λ	Learning Rate	Number of Epochs
BASEHOCK RELATHE PCMAC PBMC	LLSPIN	[1,10]	[1e-2,1e-1]	{1000, 3000, 5000, 7000, 9000}
	LSPIN	[1,10]	[1e-2,1e-1]	{1000, 3000, 5000, 7000, 9000}
	STG (l)	[1,10]	[1e-1,2e-1]	{3000, 5000, 7000, 9000}
	STG (n)	[1,10]	[1e-1,2e-1]	{3000, 5000, 7000, 9000}
	Neural Net	None	[1e-2,1e-1]	{1000, 3000, 5000, 7000, 9000}
	INVASE	{1, 5, 10}	[1e-5,1e-4]	10000
COLON	LLSPIN	[1,2]	0.1	7000
	LSPIN	[1,2]	0.05	7000
	STG (l)	[1,2]	0.5	7000
	STG (n)	[1,2]	0.5	7000
	Neural Net	None	0.1	7000
	INVASE	{1, 1.5, 2}	0.0001	10000
TOX-171	LLSPIN	[1,2]	0.1	7000
	LSPIN	[1,2]	0.05	7000
	STG (l)	[1,10]	0.5	7000
	STG (n)	[1,10]	0.5	7000
	Neural Net	None	0.1	7000
	INVASE	{1, 1.5, 2}	0.0001	10000

Table 7: Parameter settings for the neural network based methods on the real-world data. Note that INVASE uses Adam Optimizer and others use SGD optimizer. For the regularization parameter λ , the grid size for LSPIN models and STG models is 5 on BASEHOCK/RELATHE/PCMAC/PBMC datasets and 20 on COLON and TOX-171 datasets, and for INVASE model is 3 on these datasets to reduce the run time.

B.5 Cox Proportional Hazard Models for Survival Analysis Details

Here we provide details for reproduction of the example presented in Section 4.5.

B.5.1 SEER Dataset Preprocessing Steps

The data for this study was collected from the Surveillance, Epidemiology, and End Results (SEER) public datasets [46]. Female patients, ages of 25-85, diagnosed with histologically confirmed non-metastatic breast cancer between Jan 1, 2000 and Dec 31, 2016, are included. Patients with metastatic disease and those with missing data on stage, T grade, number of positive nodes, number of T nodes, vital status, and survival time are excluded. Only those patients who underwent surgery and had a known tumor size of less than 200 mm are included. Patients with bilateral breast

cancer, inflammatory disease, and *in situ* tumor are excluded. We one-hot encode the categorical variables and drop features that contain missing values. We further concatenate the data with 3 nuisance variables with values drawn from a uniform distribution $U(0,1)$. In the end, we z-score the continuous variables. In total, the data contains 538,315 patients and 55 features.

B.5.2 Training Procedures and Hyper-parameter Tuning and Settings

For the SEER data, we apply a training procedure similar to the one we applied to the BASEHOCK, RELATHE, PCMAC, PBMC datasets.

5% of each dataset is set aside as validation set. Let us denote the remaining 95% of the data as $\bar{\mathbf{X}}$. We split $\bar{\mathbf{X}}$ into 10 non-overlapping folds.

We train each model on 1 fold of $\bar{\mathbf{X}}$ and test it on the remaining non-overlapping 9 folds of $\bar{\mathbf{X}}$. The hyper-parameters are optimized on the validation set via Optuna (50 Optuna trials for the neural network methods on the learning rate and epochs as in Table 8) based on the model that was trained on a single fold and tested on the remaining 9 non-overlapping folds. These (fixed) hyper-parameters are then used in training the model on the second fold and testing it on the remaining 9 non-overlapping folds. Similarly, we use these fixed hyper-parameters to train models for folds No.3, No.4, No.5, ..., No.10, and each time test these models on the remaining 9 non-overlapping folds. We then compute the average (over the 10 folds) performance (test concordance index and number of selected features). This training and testing procedure is repeated for several regularization parameters to produce the results in the interpolation plot Fig. 5a. We note that Random Survival Forest selects almost all the features over different values of `n_estimators`, the performance of this model is presented as a single triangle shaped marker in Fig. 5a.

Parameters	Range
learning rate (all Neural Network methods)	[1e-2,1]
epochs (all Neural Network methods)	{500, 1000, 2000}
λ (COX-LLSPIN, COX-LSPIN)	[1e-9,1e-5]
λ (COX-STG(Linear/Nonlinear))	[1e-3,1e-1]
α (COX-LASSO)	[1e-7,1]
<code>n_estimators</code> (Random Survival Forest)	{1,10,100,500,1000}

Table 8: Parameter settings for different models for the survival analysis example. For COX-LLSPIN/COX-LSPIN/COX-STG, the regularization parameter is λ . For COX-LASSO, the regularization parameter is α . For Random Survival Forest, we use `n_estimators` to replace the regularization parameter. We use full batch training for all Neural Network methods.

In this example, we set the *prediction* network architecture of the nonlinear neural network methods (COX-LSPIN, COX-STG(Nonlinear), DeepSurv) to 3 hidden layers with 100, 30, and 5 neurons respectively. The linear neural network methods (COX-LLSPIN, COX-STG(Linear)) have no hidden layers. The *gating* network of LLSPIN/LSPIN is set to 1 hidden layer with 300 neurons. For the local methods including COX-LLSPIN and COX-LSPIN, the average (over the 10 folds) median (over the samples) number of selected features is reported.

C Strengths and Limitations

The proposed model leads to an interpretable prediction model that can handle datasets of low sample size (LSS). Our results demonstrate that local sparsity tied with a linear model can serve as a strong classifier on real biological datasets. Currently, the sparsity of our model is tuned via a regularization parameter λ . Increasing this parameter would decrease the average number of active features used by the model. While this encourages instance-wise sparsity, we observe that in certain cases our model still uses a large number of features (when considering the union of features over all samples). In the future, we plan to add an additional regularizer to encourage global sparsity of the model.